HHS Public Access

Author manuscript

Gene Ther. Author manuscript; available in PMC 2016 January 01.

Published in final edited form as:

Gene Ther. 2015 July ; 22(7): 568–577. doi:10.1038/gt.2015.25.

Gene delivery to the spinal cord using MRI-guided focused ultrasound

Danielle Weber-Adrian[1,2], **Emmanuel Thévenot, PhD**[1,2], **Meaghan A. O'Reilly, PhD**[3,4], **Wendy Oakden**[3,4], **Margarete K. Akens, PhD**[5,6], **Nicholas Ellens**[3,4], **Kelly Markham-Coultes**[1], **Alison Burgess, PhD**[3], **Joel Finkelstein, MD**[6,7], **Albert J.M. Yee, MD**[3,6,7], **Cari M. Whyne, PhD**[3,6,7], **Kevin D. Foust, PhD**[8], **Brian K. Kaspar, PhD**[8], **Greg J. Stanisz, PhD**[3,4], **Rajiv Chopra, PhD**[3,4,9], **Kullervo Hynynen**[3,4], and **Isabelle Aubert, PhD**[*,1,2]

[1]Brain Sciences, Biological Sciences, Sunnybrook Research Institute, Toronto, ON Canada

[2]Department of Laboratory Medicine and Pathobiology, University of Toronto, Toronto, ON Canada

[3]Physical Sciences, Sunnybrook Research Institute, Toronto, ON, Canada

[4]Department of Medical Biophysics, University of Toronto, Toronto, ON, Canada

[5]TECHNA Institute, University Health Network, Toronto, ON Canada

[6]Department of Surgery, University of Toronto, Toronto, ON, Canada

[7]Centre for Spinal Trauma, Division of Orthopaedic Surgery, Sunnybrook Research Institute, Toronto, ON Canada

[8]Department of Neuroscience, Ohio State University and Center for Gene Therapy, The Research Institute at Nationwide Children's Hospital, Columbus, OH, USA

[9]Department of Radiology, University of Texas Southwestern Medical Center, Dallas, TX, USA

Abstract

Non-invasive gene delivery across the blood-spinal cord barrier (BSCB) remains a challenge for treatment of spinal cord injury or disease. Here, we demonstrate the use of magnetic resonance imaging-guided focused ultrasound (MRIgFUS) to mediate non-surgical gene delivery to the spinal cord, using self-complementary adeno-associated virus serotype 9 (scAAV9). scAAV9 encoding green fluorescent protein (GFP) was injected intravenously in rats. MRIgFUS allows for transient, targeted permeabilization of the BSCB through the interaction of FUS with systemically-injected Definity® lipid-shelled microbubbles. scAAV9-GFP was delivered at 3 dosages: 4×10^8, 2×10^9, and 7×10^9 vector genomes per gram (VG/g). Viral delivery at 2×10^9 and 7×10^9 VG/g leads to robust GFP expression in the targeted length and side of the spinal cord. At a dose of 2×10^9 VG/g, GFP expression was found in 36% of oligodendrocytes, and in 87% of

[*]Corresponding Author: Isabelle Aubert, isabelle.aubert@sri.utoronto.ca, Phone: (416) 480-5831 Fax: (416) 480-5737, Sunnybrook Research Institute, 2075 Bayview Ave, S112, Toronto, ON, Canada M4N 3M5.

Conflict of Interest: The authors declare no conflict of interest.

neurons in FUS-treated areas. FUS applications to the spinal cord could address a long-term goal of gene therapy: delivering vectors from the circulation to diseased areas in a noninvasive manner.

Keywords

AAV; adeno-associated virus; GFP; green-fluorescent protein; MRIgFUS; non-invasive gene delivery

Introduction

Gene therapy has entered clinical trials for the treatment of neurodegenerative disorders and chronic pain,[1] and has shown promise in preclinical animal models for the treatment of spinal cord injury (SCI),[2,3] spinal muscular atrophy,[4-7] and amyotrophic lateral sclerosis (ALS).[3,8] Gene therapy directed to the central nervous system (CNS) could realize its full potential upon the development of safe and effective delivery methods capable of targeting gene transfer to the desired location non-invasively.

Both the blood -brain barrier (BBB) and the blood-spinal cord barrier (BSCB) are characterized by the presence of tight junctions and reduced active transport.[9] Large molecules (>500 Da) of low lipid solubility, and with no active transporter, do not readily pass the BBB and BSCB.[10] The development of non-invasive approaches to increase the delivery of therapeutics from the blood to the brain and spinal cord has been an area of great research interest.

Transcranial focused ultrasound (FUS), when used in conjunction with systemically circulating microbubbles,[11] has the ability to transiently open the BBB causing a downregulation of tight-junctional proteins (e.g. ZO-1, claudin-1, claudin-5, occludin),[12-14] and an upregulation of active transport proteins such as caveolin-1.[15,16] This permeabilization is transient, lasting for approximately 4-6 h after sonication.[17] FUS-mediated BBB disruption has been used to deliver large agents, such as antibodies (∼150 kDa),[18-20] viral vectors (∼20 nm)[21,22] and stem cells (8-10 μm)[23] to targeted brain areas. Positive therapeutic response to agents delivered using FUS BBB disruption has been observed in mouse models of cancer[24] and neurodegenerative diseases.[20,25] Additionally, previous studies show that microbubble-mediated FUS treatment alone increases adult neurogenesis and dendritic plasticity.[26,27]

FUS-mediated BSCB opening has the potential to facilitate drug, cell and gene therapies for spinal cord ailments such as tumors, injury, or diseases like ALS. However, ultrasound can be scattered by heterogeneous materials such as bone, and the complexity of the vertebrae represents a challenge for the translation of FUS-mediated BSCB opening to the spinal cord.[28,29] Advances in the field have led to a preliminary investigation demonstrating the feasibility of transient opening of the BSCB.[30] Here, we demonstrate FUS-mediated BSCB opening in a rat model under magnetic resonance imaging (MRI)-guidance and its application for gene delivery using self-complementary adeno-associated virus serotype 9 (scAAV9).

Results

FUS treatments were performed with an ultrasound transducer located below the animal placed in dorsal recumbency, producing BSCB disruption at the level of the cervical spine (Figure 1a and b). scAAV9-GFP was injected intravenously at doses of 4×10^8, 2×10^9 and 7×10^9 vector genomes per gram (VG/g). Contrast-enhanced MRI was used to target the spine (Figure 1c) and confirm the increase in BSCB permeability post-FUS treatment (Figure 1d and e). Immunohistochemistry data were obtained from longitudinal and transverse sections of the FUS-targeted area (Figure 1f).

MRI-guided focused ultrasound (MRIgFUS) treatment was successful inmediating gene delivery of scAVV9-GFP,administered intravenously at 2 and 7×10^9 VG/g, to the unilateral targeted region of the spinal cord (Figure 2). This resulted in GFP expression in oligodendrocytes (Figure 3) and neurons (Figure 4). At a dose of 2×10^9 VG/g scAAV9-GFP, we found that 36% of oligodendrocytes and 87% of neurons expressed GFP in FUS-targeted areas of the spinal cord. GFP expression was evident in the liver, minimal in the heart, and marginally detected in the muscle (Figure 5).

MRI-Enhancement and Blood-Spinal Cord Barrier Permeability

1.5TMRI was used to visualize and target the cervical area of the spinal cord (Figure 1c). Following FUS treatment, BSCB opening was confirmed by the entry of MRI contrast agent in localized areas of the spinal cord (Figure 1d, arrows). Using these FUS parameters, enhancement in the soft tissue surrounding the targeted spinal cord was occasionally noted (Figure 1d). In order to assess long-term safety of MRIgFUS treatment, 2 animals were reimaged using 7T MRI 13 days post treatment (Figure 1e). No indications of fluid retention, or structural abnormalities were observed on MRI (Supplementary Figure 1a).

In 11 out of the 12 rats treated, tissue collected 13 days post treatment showed no signs of red blood cell infiltration, damage, or other histopathological abnormalities at the gross anatomy level (Supplementary Figure 1b). The temperature of liquid-lipid suspension used to form the microbubbles through mechanical agitation has been shown to affect bubble size distribution, and at lower temperatures results in the formation of larger bubbles.[31] We found that in one animal treated at the same FUS parameters, but with microbubbles pre-activated at approximately 4°C, as opposed to room temperature, resulted in damage of the spinal cord. After FUS treatment, this animal demonstrated front limb paresis, and 7T MRI imaging, performed 13 days post treatment, showed significant structural abnormalities in the spinal cord tissue (Supplementary Figure 1c). Hematoxylin and eosin stained sections from the FUS-treated area of this animal showed damage (Supplementary Figure 1d). There were no clinical symptoms in the remaining 11 animals post treatment with microbubbles at room temperature.

Gene Expression Following Unilateral MRIgFUSscAAV9-GFP Delivery to the Spinal Cord

This experiment aimed to establish that MRIgFUS could be used to target one side of the cervical spinal cord in adult rats and deliver systemically-injected scAAV9-GFP to that FUS-treated location, where GFP would then be expressed.

At the lowest dose of scAAV9-GFP (4×10^8 VG/g), low levels of GFP expression were detected as illustrated in a longitudinal spinal cord section (Figure 2a), and transverse section of the targeted area (Figure 2b and c). GFP expression was below detection levels on the contralateral side (Figure 2d). At the middle dose of scAAV9-GFP (2×10^9 VG/g), strong GFP expression was observed in longitudinal (Figure 2e), and transverse sections of the spinal cord within the FUS-treated area (Figure 2f). At higher magnification, GFP expression is evident on the treated side (Figure 2g), but not the contralateral side (Figure 2h). At the highest dose of scAAV9-GFP (7×10^9 VG/g), the longitudinal (Figure 2i) and transverse views (Figure 2j) of the FUS-treated area of the spinal cord showed the most abundant GFP expression compared to the middle and low doses. At higher magnification, GFP is more prominent on the treated side (Figure 2k) than on the contralateral side (Figure 2l).

scAAV9-MediatedGFP Expression by Oligodendrocytes

In order to assess which cell types within the spinal cord express GFP after delivery of scAAV9-GFP with MRIgFUS, tissue samples were stained with oligodendrocyte lineage transcription factor 2 (Olig2). At the lowest dose of scAAV9-GFP (4×10^8 VG/g), GFP expression in Olig2-positive cells was not detected (Figure 3a-c). At the middle dose (2×10^9 VG/g), GFP expression was abundant (Figure 3d) and present in some Olig2-positive cells (Figure 3e and f, arrow). At this dose, 36± 3 % (mean ± SD, n=4) of Olig2-positive cells in FUS-treated regions of the spinal cord, were GFP-positive. At the highest dose (7×10^9 VG/g), GFP expression in the targeted area of the spinal cordwas increased compared to the low and middle dose (Figure 3g-i).

scAAV9 Mediated GFP Expression by Neurons

For assessment of GFP expression in neurons, tissue sections were stained with antibodies against the neuronal nuclear antigen (NeuN), and choline acetyltransferase (ChAT). Images were taken within the ventral horn of transverse sections from the treated cervical spine. At the lowest dose of scAAV9-GFP (4×10^8 VG/g), GFP expression was below detection levels in NeuN-positive (blue) and ChAT-positive (red) neurons (Figure 4a-e) Conversely, at the middle (2×10^9 VG/g; Figure 4f-j) and high (7×10^9 VG/g; Figure 4k-o) doses of scAAV9-GFP, ChAT- and NeuN-positive cells were found to express GFP (Figure 4h-j and m-o, arrows). At 2×10^9 VG/g scAAV9-GFP, 87%±4% (mean ± SD, n=4) of NeuN-positive cells were GFP-positive in FUS-treated areas. Few cells positive for NeuN and weakly stained for ChAT did not express significant levels of GFP (Figure 4m-o, arrowheads). GFP expression was restricted to the FUS-treated side at 2×10^9 and 7×10^9 VG/g,and under the same imaging parameters, no background was detected on the contralateral side with no FUS treatment (Figure 4a′-c′; f′-h′; k′-m′).

scAAV9-Mediated GFP Expression in Peripheral Organs

GFP expression was evaluated in peripheral organs and in the brain after tail vein injection of scAAV9-GFP, paired with MRIgFUS targeted to the spinal cord. GFP expression within the liver, heart, and muscle was evaluated (Figure 5). The highest level of GFP expression was seen in the liver (Figure 5a), whereas the fluorescence signal in the heart (Figure 5b) at the same confocal parameters was considerably lower. GFP expression in the muscle tissue

(Figure 5c) when evaluated at these same confocal parameters was undetectable (data not shown). For this reason, the GFP signal in muscle tissue was enhanced using a GFP antibody coupled to Cy3, and confocal settings were optimized for the detection of this fluorochrome (Figure 5c). GFP expression was not detected in the kidney or brain, despite signal enhancement with GFP antibody (data not shown). Topro3 iodide was used as a nuclear stain.

Discussion

Direct injection of therapeutic agents into the spinal cord carries the risks of complication due to needle placement, infection, nerve trauma, air embolism, disc entry, hematoma, and hypersensitivity reaction.[32] Using MRIgFUS, delivery of therapeutic agents to the spinal cord can be done non-surgically, greatly reducing the risks associated with direct injection. The current study is a proof -of -concept that MRIgFUS can be used for non-invasive gene delivery to the spinal cord. Briefly, a viral vector carrying a reporter protein (scAAV9-GFP) was injected intravenously and MRIgFUS was used to target one side of the cervical spinal cord in adult rats, delivering the transgene across the BSCB at that location.

Systemic injection of AAV9 is an efficient method for gene delivery to the spinal cord in neonate rodents[33]. This is due to the properties of the neonatal BSCB, which does not fully mature until approximately 14 days after birth.[34,35] In animals with a mature BSCB, the dose of AAV9 injected intravenously needs to be much higher to effectively permeate the BSCB and reach the spinal cord (e.g. 4×10^{12} DNAse resistant particles;[36] and 1×10^{11} VG/g).[37] Here, we show that the use of MRIgFUS, as a means to increase BSCB permeability, decreased the dose required for gene delivery to the spinal cord to 2×10^{9} VG/g, representing a 50-fold reduction from the previously reported minimumvalues.[37] FUS-mediated gene delivery could therefore provide an alternative or compliment to current intrathecal and intravascular strategies.[7]

As observed in the mouse brain,[21] FUS-mediated gene delivery to the spinal cord did not influence the tropism of scAAV9 towards a particular cell type. scAAV9-GFP injected intravenously at 2 and 7×10^{9} VG/g and combined with MRIgFUS, resulted in GFP expression in neurons, including ChAT-positive motor neurons, oligodendrocytes. Previous studies using higher dosages of intravenous AAV9, but without FUS, have shown gene transfer in a maximum of 28% of motor neurons,[37] and 7% of oligodendrocytes.[38] In addition, intravenous delivery of scAAV9 was shown to result in GFP expression in cells that were neither NeuN-positive, nor Olig2 positive. Previous studies suggest that these cells may be astrocyte-perivascular endfeet,[36] orendothelial cells, which the virus would have been exposed to while crossing the BSCB.[39] Identification of other GFP-positive cell types will be evaluated in future studies.

In addition to reducing the required effective dose of scAAV9 for gene delivery, MRIgFUSis able to target a localized area or side of the spinal cord. This is of significant value towards the design of therapeutic approaches for spinal cord disorders or injury. Additionally, the ability to target one side of the spinal cord could eventually be used for the treatment of hemisection lesions, such as in Brown-Séquard syndrome,[40] in that a

therapeutic agent could be non-invasively delivered to only the injured side of the spinal cord. The non-FUS targeted areas of the spinal cord in our study showed no GFP expression, allowing us to conclude that the delivery of the vector was mediated by MRIgFUS and not by the innate ability of scAAV9 to cross the BSCB. Furthermore, the lack of GFP expression in the brain indicates that scAAV9, at the doses tested, did not cross the BBB in an appreciable amount.

In order to assess gene expression in peripheral organs, the liver, kidney, quadriceps muscle, and heart tissue were analyzed, with only the liver, heart, and muscle showing GFP expression. These results are in agreement with previous studies in rats that found systemic scAAV9 delivery resulted in gene expression in the liver,[41] and heart.[41,42] Studies investigating the systemic delivery of scAAV9 in mice also found abundant gene expression in skeletal muscle with some expression in the kidney.[21,36,37] Our study is consistent with the findings that scAAV9 delivery does not result in significant gene expression in the rat kidney.[41] This variance in gene expression by peripheral organs in mice and rat studies can be due to the dosages, preparations of scAAV9,and potential interspecies differences in cell surface expression of terminal N-linked galactose, which is the primary receptor for AAV9.[43] One strategy that could be implemented to decrease peripheral gene expression would be the use of neural-specific promoters. In the case of scAAV9, there have been significant differences observed in motor neuron gene delivery after intrathecal injection in mice, when the promoter was varied between a cytomegalovirus promoter (CMV) or a chicken-β-actin (CBA) promoter, with scAAV9-CMV inducing the greatest amount of gene expression in motor neurons.[44] By varying the promoter, further regulation of gene expression after MRIgFUS-mediated gene delivery may be possible.

With regards to the animal which experienced post-treatment spinal cord injury, it has been shown that pre-activation vial temperature effects microbubble size distribution.[31] Definity® microbubbles are activated by mechanical agitation, which generates bubbles from a vial containing an aqueous solution of lipids with octofluoropropane gas; vials activated at a colder temperature produce a greater number of larger bubbles.[31] Larger microbubbles can result in greater barrier opening.[45] The histology results of the remaining 11 animals, treated at the same FUS parameters, showed no signs of tissue damage, which further suggests that the injury seen in the first animal was caused by larger microbubbles, generated through activation of the vial at a lower temperature. A recent study that used FUS to intentionally generate a spinal cord injury model in rats, demonstrated that FUS applied at an acoustic power of at least 1.3-1.6 W in the presence of microbubbles would result in such damage.[46] When the acoustic power is limited to 0.73 W, as it was here, there was no evidence of spinal cord damage, when using microbubbles brought to room temperature before activation. The MRI enhancement in soft tissue immediately surrounding the FUS-treated area of the spinal cord is due to the small size of the animal relative to the focal characteristics of the transducer used in this study. In a clinical setting, a wider aperture transducer could be used, which would allow for a tighter focal spot.[47] To provide additional safety to FUS-mediated BSCB opening, real-time monitoring techniques developed to tune the exposure parameters for a controlled BBB opening in transcranial FUS treatment[48,49] could be adapted for application to the spinal cord.

Finally, it is known that FUS alone in other regions of the CNS can enhance neurogenesis, dendritic complexity [26,27] and glial activation.[25] Therefore, it will be of interest to evaluate the impact of FUS alone on neuronal and glial plasticity in the spinal cord, and assess the long-term benefits or risks of such potential remodeling.

In summary, an intravenous dose of 2×10^9 VG/g was sufficient for targeted delivery of scAAV9-GFP to the rat cervical spinal cord, resulting in significant gene expression in 87% of neurons and 36% of oligodendrocytes in the FUS-targeted region. MRIgFUS has the potential to be further developed for targeted, non-invasive gene therapy to the spinal cord.

Materials and Methods

Animals

This experiment used 12, approximately 300g-male Wistar rats (Charles River, Canada). All of the animal procedures were carried out in compliance with the Canadian Council on Animal Care and the Animals for Research Act of Ontario guidelines, and with the approval of the Sunnybrook Research Institute Animal Care Committee.

Virus

scAAV9 was produced using a transient transfection procedure and a double-stranded AAV2-ITR-based CB promoter-green fluorescent protein (GFP) vector, with a plasmid encoding Rep2Cap9 sequence as previously described,[36] as well as an adenoviral helper plasmid pHelper (Stratagene, Santa Clara, CA). The vector was then sequenced to verify that it was identical to that of the previously described AAV serotype 9. Vector purification was done with two cesium chloride density gradient purification steps, dialyzation against phosphate-buffered saline (PBS), and formulation with 0.001% Pluronic-F68 to prevent virus aggregation, before storage at 4°C.[36] Viral preparations were titered via quantitative-PCR and Taq-Man technology. The vector purity was analyzed via 4–12% sodium dodecyl sulfate-acrylamide gel electrophoresis and silver staining (Invitrogen, Carlsbad, CA).

The 3 dosages of scAAV9-GFP used for this study were 4×10^8 (n=4), 2×10^9(n=6) and 7×10^9 (n=2) VG/g of treated animal.

MRIgFUS

Rats were anesthetized with isofluorane, and then with an additional mixture of ketamine (40-50 mg/kg) and xylazine (10 mg/kg) delivered via intramuscular injection. The hair was removed from the neck and back using an electric razor followed by depilatory cream. A 22G angio-catheter was placed in the tail vein to facilitate delivery of microbubbles and the MRI contrast agent. Animals were placed in dorsal recumbency on the top plate of a three-axis positioner, operationally similar to that described by Chopra *et al*,[50] with their necks contacting a water bath. The ultrasound transducer was located on a positioning arm below the animal (Figure 1a).

Animals were imaged using a 1.5T MRI (1.5T Signa, General Electric, Milwaukee, WI). Pre-treatment T2 weighted images were used for selecting the ultrasound targets. Contrast-enhanced baseline T1 weighted images were captured before sonication (Figure 1c). The

cervical spine was selected for targeting to minimize MRI artifacts from heart motion. Ultrasound was generated using a 1.114 MHz spherically focused transducer (Aperture: 7 cm, F-number: 0.8), driven using a function generator and radio frequency (RF) power-amplifier. Sonications consisted of 10 ms ultrasound bursts at a repetition rate of 0.5 Hz, for a total of 5 min, targeted to the cervical spine. The acoustic power during the burst was kept below inertial cavitation threshold (based on earlier experiments) and set to 0.73 W. Definity microbubbles (0.02 ml/kg, Lantheus Medical Imaging) were injected into the tail vein catheter at the start of the sonication, followed by 0.5 ml saline. During each sonication, 6 spots were sonicated at 1 mm spacing to produce a band of BSCB opening in the cervical spine (Figure 1b). Gadodiamide (0.2 ml/kg Omniscan, GE Healthcare) contrast-enhanced T1 weighted images were captured post FUS to assess the permeability of the BSCB (Figure 1d). Some animals received a second sonication if the first did not result in BSCB opening, as assessed by MRI enhancement.

5-30 min following ultrasound treatment, rats received an injection of 0.3 ml of viral solution via tail vein catheter, followed by 0.5 ml of saline to clear the catheter of any residual virus and ensure transfer into the bloodstream. After recovery, rats were returned to individual cages for 13 days.

High Resolution MRI

Images were acquired using a 7T Bruker Biospin (Bruker BioSpin MRI GmbH, Ettlingen, Germany) post FUS, at a resolution of 0.15 × 0.15 mm/pixel, and 1 mm slice thickness in order to more precisely localize BSCB opening. Contrast enhanced axial images were acquired using a 2D FLASH sequence, (TE 2.47ms, TR 200ms, 10 averages, FA 65°, resolution 0.15×0.15 mm/pixel, 1mm slice thickness). Six of the animals were imaged immediately following ultrasound treatment (Figure 1e), and 2 of these animals were imaged 13 days post treatment to confirm that the BSCB was no longer permeable (Supplementary Figure 1a).

Histological processing

13 days after FUS treatment, rats were deeply anesthetized with ketamine (75 mg/kg) and xylazine (10 mg/kg), and transcardially perfused with 0.9% saline solution, followed by 4% paraformaldehyde (PFA) in 0.1M PO_4 The spinal cord, brain, and organs including: heart, kidney, quadriceps muscle and liver, were collected and post fixed in 4% PFA solution for 24h, and stored at 4°C in 30% sucrose solution. Spinal cord sections were cut in either transverse or longitudinal orientation on a vibratome at room temperature. The distance to the treatment area was estimated, in millimeters from the brain stem, using the MRI enhancement images and ImageJ software. For transverse sections, each spine was first sectioned into 8, 3 mm-thick pieces, with the 4th piece (P4) representing the treatment target area (Figure 1f). Then 12, 50 μm-thick sections were cut from the top of each piece for analysis. The bottom of each piece was marked with blue tissue dye (Davidson Marking System, Bradley Products, 1013-5, Bloomington, MN, USA) to indicate orientation. The brain and peripheral organs were mounted onto a sliding microtome with Tissue-Tek OCT and frozen with dry ice for cutting into 40 μm-thick sections. Sections were stored at -20°C in cryoprotective glycerol solution.

Histology

Hematoxylin and eosin (H&E) staining was used on 50 μm-thick (n=11) and 5 μm-thick (n=7) spinal cord sections as previously described.[51,52] 50 μm, free floating sections were mounted on paraffin-coated microscope slides and allowed to adhere for 72 h, before staining by standard H&E procedures. Tissue integrity of the spinal cord in 11 animals was assessed from both within and outside the targeted region.

Immunohistochemistry

Free-floating spinal cord sections were washed 3 times for 10 min in PBS, and incubated for 1 h in blocking solution containing PBS with 10% donkey serum and 0.4% Triton X100 (PBS++). Sections were then incubated for 72 h at 4°C in rabbit anti-GFP (1:500, Millipore, AB3080, Bedford, MA, USA), mouse anti-oligodendrocyte lineage transcription factor 2 (Olig2)(1:500, Millipore, MABN50), mouse anti-neuronal nuclear antigen (NeuN)(1:500, Millipore, MAB377), or goat anti-choline acetyltransferase (ChAT)(1:100, Millipore, AB144P) diluted in PBS++. The sections were then washed 3 times for 10 min in PBS. This was followed by incubation at room temperature for 1 h in the following secondary antibodies in PBS++: Biotin-conjugated donkey anti-rabbit IgG (1:80 Jackson ImmunoResearch, 711-065-152, West Grove, PA, USA), Cy3-conjugated donkey anti-goat IgG (1:200, Jackson ImmunoResearch, 705-165-147), and Cy5-conjugated donkey anti-mouse IgG (1:200, Jackson ImmunoResearch, 715-175-150). After washing the sections twice for 10 min in PBS, they were incubated at room temperature in PBS++ with Alexa488-conjugated Streptavidin (1:200, Jackson ImmunoResearch, 016-540-084) for 2 h. After washing 3 times in PBS, sections were rinsed in 0.1M PO_4 and mounted on a microscope slide with polyvinyl alcohol and 1,4-diazabicyclo[2.2.2]octane (PVA-DABCO) and a coverslip.

40 μm-thick brain, heart, and quadriceps muscle sections were washed 3 times in tris-buffered saline (TBS) for 10 min, before a 1 h incubation in blocking solution (TBS, donkey serum 7.5%, and triton X-100 0.5%) at room temperature. Sections were incubated in rabbit anti-GFP antibody (1:500, AB3080, Millipore) in blocking solution overnight at 4°C. Sections were washed 2 times with TBS for 15 min before a 2 h incubation with donkey anti-rabbit IgG biotin (1:500, Jackson ImmunoResearch, 711-065-152), diluted in blocking solution. After two 15 min washes in TBS, the sections were incubated with Cy3-conjugated Streptavidin (1:500, Jackson ImmunoResearch, 016-160-084) and Topro3 iodide (1:500, Invitrogen, T3605, Eugene, OR, USA) for 2 h at room temperature. Sections were then rinsed 3 times in TBS, and once in 0.1M PO_4 before mounting on a microscope slide with PVA-DABCO and a coverslip.

Liver and kidney sections, of 40 μm thickness, were washed 3 times for 10 min in TBS, and then incubated for 1 h in blocking solution at room temperature. Sections were then incubated with Topro3 iodide (1:500, Invitrogen, T3605) in blocking solution at room temperature for 2 h. The sections were rinsed 3 times in TBS, and once in 0.1M PO_4 before mounting on a microscope slide with PVA-DABCO and a coverslip.

Imaging

Images of spinal cord in Figure 2a, b, e, f, i, j were acquired using an Axioplan 2 imaging system (Carl Zeiss, Toronto, ON). Series of adjacent images were captured using a 10× objective, which were then assembled into a single mosaic with Virtual Slice (Stereo Investigator; Bioscience, Williston, VT, USA).

All other images were taken using either a Zeiss Axiovert 100/LSM 510, Zeiss Axio Observer Z1/LSM 700 or a Zeiss Z1 Observer/Yokogawa Spinning Disk (Carl Zeiss, Toronto, ON) microscope. Excitation wavelengths of 488nm (GFP), 561nm (Cy3), and 633nm (Cy5) were used. Spinal cord images are shown as single confocal plane. Liver, muscle, and heart images as shown are a projection of five, 1.13 μm Z-stacks. Image montages were prepared with Adobe Photoshop CS5 (Adobe Systems Incorporated).

Cell Counts

The percentages of Olig2-positive and NeuN-positive cells expressing GFP were quantified under stereology-based principles using Stereo Investigator™ (MBF Biosciences) on a Zeiss AxioImager M2 microscope. Three representative sections at the FUS-treated level of the spinal cordfrom animals receiving 2×10^9 VG/g (n=4) were used. Quantification was done with a 63× oil objective, using the optical fractionator probe, from z stacks collected following systematic, random sampling. Regions of interest were at the FUS-treated level and included visible areas of GFP expression in the spinal cord at 5× magnification. The average coefficient of error (Gundersen m=1) was 0.04 for the number of Olig2-positive cells expressing GFP, and 0.06 for the number of NeuN-positive cells expressing GFP.

Supplementary Material

Refer to Web version on PubMed Central for supplementary material.

Acknowledgments

Support for this work was provided by the Centre for Spinal Trauma, Sunnybrook Health Sciences Centre, CIHR FRN 93603 (IA), NIH grant R01-EB003268 (KH), and the Canada Research Chair Program (KH). The authors thank Dr. Paul Nagy for helping to edit this manuscript. The authors also wish to thank Dr. Julie Korich, and MBF Biosciences for their counsel in regards to cell counting.

References

1. Goins WF, Cohen JB, Glorioso JC. Gene therapy for the treatment of chronic peripheral nervous system pain. Neurobiol Dis. 2012 Nov; 48(2):255–270. [PubMed: 22668775]
2. Romero MI, Rangappa N, Garry MG, Smith GM. Functional regeneration of chronically injured sensory afferents into adult spinal cord after neurotrophin gene therapy. J Neurosci. 2001 Nov 1; 21(21):8408–8416. [PubMed: 11606629]
3. Nagahara AH, Tuszynski MH. Potential therapeutic uses of BDNF in neurological and psychiatric disorders. Nat Rev Drug Discov. 2011 Mar; 10(3):209–219. [PubMed: 21358740]
4. Passini MA, Bu J, Roskelley EM, Richards AM, Sardi SP, O'Riordan CR, et al. CNS-targeted gene therapy improves survival and motor function in a mouse model of spinal muscular atrophy. J Clin Invest. 2010 Apr; 120(4):1253–1264. [PubMed: 20234094]

5. Foust KD, Wang X, McGovern VL, Braun L, Bevan AK, Haidet AM, et al. Rescue of the spinal muscular atrophy phenotype in a mouse model by early postnatal delivery of SMN. Nat Biotechnol. 2010 Mar; 28(3):271–274. [PubMed: 20190738]
6. Bevan AK, Duque S, Foust KD, Morales PR, Braun L, Schmelzer L, et al. Systemic gene delivery in large species for targeting spinal cord, brain, and peripheral tissues for pediatric disorders. Mol Ther. 2011 Nov; 19(11):1971–1980. [PubMed: 21811247]
7. Meyer K, Ferraiuolo L, Schmelzer L, Braun L, McGovern V, Likhite S, et al. Improving Single Injection CSF Delivery of AAV9-mediated Gene Therapy for SMA: A Dose-response Study in Mice and Nonhuman Primates. Mol Ther. 2014 Oct 31.
8. Lepore AC, Haenggeli C, Gasmi M, Bishop KM, Bartus RT, Maragakis NJ, et al. Intraparenchymal spinal cord delivery of adeno-associated virus IGF-1 is protective in the SOD1G93A model of ALS. Brain Res. 2007 Dec 14.1185:256–265. [PubMed: 17963733]
9. Reese TS, Karnovsky MJ. Fine structural localization of a blood-brain barrier to exogenous peroxidase. J Cell Biol. 1967 Jul; 34(1):207–217. [PubMed: 6033532]
10. Pardridge WM. Blood-brain barrier delivery. Drug Discov Today. 2007 Jan; 12(1-2):54–61. [PubMed: 17198973]
11. Hynynen K, McDannold N, Vykhodtseva N, Jolesz FA. Noninvasive MR imaging-guided focal opening of the blood-brain barrier in rabbits. Radiology. 2001 Sep; 220(3):640–646. [PubMed: 11526261]
12. Sheikov N, McDannold N, Sharma S, Hynynen K. Effect of focused ultrasound applied with an ultrasound contrast agent on the tight junctional integrity of the brain microvascular endothelium. Ultrasound Med Biol. 2008 Jul; 34(7):1093–1104. [PubMed: 18378064]
13. Zhang Z, Xue Y, Liu Y, Shang X. Additive effect of low-frequency ultrasound and endothelial monocyte-activating polypeptide II on blood-tumor barrier in rats with brain glioma. Neurosci Lett. 2010 Aug 30; 481(1):21–25. [PubMed: 20600613]
14. Fan L, Liu Y, Ying H, Xue Y, Zhang Z, Wang P, et al. Increasing of blood-tumor barrier permeability through paracellular pathway by low-frequency ultrasound irradiation in vitro. J Mol Neurosci. 2011 Mar; 43(3):541–548. [PubMed: 21104456]
15. Xia CY, Zhang Z, Xue YX, Wang P, Liu YH. Mechanisms of the increase in the permeability of the blood-tumor barrier obtained by combining low-frequency ultrasound irradiation with small-dose bradykinin. J Neurooncol. 2009 Aug; 94(1):41–50. [PubMed: 19234812]
16. Deng J, Huang Q, Wang F, Liu Y, Wang Z, Wang Z, et al. The role of caveolin-1 in blood-brain barrier disruption induced by focused ultrasound combined with microbubbles. J Mol Neurosci. 2012 Mar; 46(3):677–687. [PubMed: 21861133]
17. Hynynen K, McDannold N, Vykhodtseva N, Raymond S, Weissleder R, Jolesz FA, et al. Focal disruption of the blood-brain barrier due to 260-kHz ultrasound bursts: a method for molecular imaging and targeted drug delivery. J Neurosurg. 2006 Sep; 105(3):445–454. [PubMed: 16961141]
18. Kinoshita M, McDannold N, Jolesz FA, Hynynen K. Targeted delivery of antibodies through the blood-brain barrier by MRI-guided focused ultrasound. Biochem Biophys Res Commun. 2006 Feb 24; 340(4):1085–1090. [PubMed: 16403441]
19. Raymond SB, Treat LH, Dewey JD, McDannold NJ, Hynynen K, Bacskai BJ. Ultrasound enhanced delivery of molecular imaging and therapeutic agents in Alzheimer's disease mouse models. PLoS One. 2008 May 14.3(5):e2175. [PubMed: 18478109]
20. Jordao JF, Ayala-Grosso CA, Markham K, Huang Y, Chopra R, McLaurin J, et al. Antibodies targeted to the brain with image-guided focused ultrasound reduces amyloid-beta plaque load in the TgCRND8 mouse model of Alzheimer's disease. PLoS One. 2010 May 11.5(5):e10549. [PubMed: 20485502]
21. Thevenot E, Jordao JF, O'Reilly MA, Markham K, Weng YQ, Foust KD, et al. Targeted delivery of self-complementary adeno-associated virus serotype 9 to the brain, using magnetic resonance imaging-guided focused ultrasound. Hum Gene Ther. 2012 Nov; 23(11):1144–1155. [PubMed: 22838844]

22. Grimm D, Kay MA. From virus evolution to vector revolution: use of naturally occurring serotypes of adeno-associated virus (AAV) as novel vectors for human gene therapy. Curr Gene Ther. 2003 Aug; 3(4):281–304. [PubMed: 12871018]

23. Burgess A, Ayala-Grosso CA, Ganguly M, Jordao JF, Aubert I, Hynynen K. Targeted delivery of neural stem cells to the brain using MRI-guided focused ultrasound to disrupt the blood-brain barrier. PLoS One. 2011; 6(11):e27877. [PubMed: 22114718]

24. Chen L, Mu Z, Hachem P, Ma CM, Wallentine A, Pollack A. MR-guided focused ultrasound: enhancement of intratumoral uptake of [(3)H]-docetaxel in vivo. Phys Med Biol. 2010 Dec 21; 55(24):7399–7410. [PubMed: 21098923]

25. Jordao JF, Thevenot E, Markham-Coultes K, Scarcelli T, Weng YQ, Xhima K, et al. Amyloid-beta plaque reduction, endogenous antibody delivery and glial activation by brain-targeted, transcranial focused ultrasound. Exp Neurol. 2013 Oct.248:16–29. [PubMed: 23707300]

26. Scarcelli T, Jordao JF, O'Reilly MA, Ellens N, Hynynen K, Aubert I. Stimulation of hippocampal neurogenesis by transcranial focused ultrasound and microbubbles in adult mice. Brain Stimul. 2014 Mar-Apr;7(2):304–307. [PubMed: 24629831]

27. Burgess A, Dubey S, Yeung S, Hough O, Eterman N, Aubert I, et al. Alzheimer's Disease in a Mouse Model: MR Imaging guided Focused Ultrasound Targeted to the Hippocampus Opens the Blood-Brain Barrier and Improves Pathology and Behavior. Radiology. 2014 in press.

28. Fry FJ, Barger JE. Acoustical properties of the human skull. J Acoust Soc Am. 1978 May; 63(5): 1576–1590. [PubMed: 690336]

29. Kaufman JJ, Einhorn TA. Ultrasound assessment of bone. J Bone Miner Res. 1993 May; 8(5):517–525. [PubMed: 8511979]

30. Wachsmuth J, Chopra R, Hynynen K. Feasibility of Transient Image-guided Blood-Spinal Cord Barrier Disruption. AIP Conference Proceedings. 2009; 1113(1):256–259.

31. Helfield BL, Huo X, Williams R, Goertz DE. The effect of preactivation vial temperature on the acoustic properties of Definity. Ultrasound Med Biol. 2012 Jul; 38(7):1298–1305. [PubMed: 22502892]

32. Goodman BS, Posecion LW, Mallempati S, Bayazitoglu M. Complications and pitfalls of lumbar interlaminar and transforaminal epidural injections. Curr Rev Musculoskelet Med. 2008 Dec; 1(3-4):212–222. [PubMed: 19468908]

33. Dominguez E, Marais T, Chatauret N, Benkhelifa-Ziyyat S, Duque S, Ravassard P, et al. Intravenous scAAV9 delivery of a codon-optimized SMN1 sequence rescues SMA mice. Hum Mol Genet. 2011 Feb 15; 20(4):681–693. [PubMed: 21118896]

34. Vorbrodt AW, Dobrogowska DH, Tarnawski M. Immunogold study of interendothelial junction-associated and glucose transporter proteins during postnatal maturation of the mouse blood-brain barrier. J Neurocytol. 2001 Aug; 30(8):705–716. [PubMed: 12118158]

35. Vannucci SJ. Developmental expression of GLUT1 and GLUT3 glucose transporters in rat brain. J Neurochem. 1994 Jan; 62(1):240–246. [PubMed: 8263524]

36. Foust KD, Nurre E, Montgomery CL, Hernandez A, Chan CM, Kaspar BK. Intravascular AAV9 preferentially targets neonatal neurons and adult astrocytes. Nat Biotechnol. 2009 Jan; 27(1):59–65. [PubMed: 19098898]

37. Duque S, Joussemet B, Riviere C, Marais T, Dubreil L, Douar AM, et al. Intravenous administration of self-complementary AAV9 enables transgene delivery to adult motor neurons. Mol Ther. 2009 Jul; 17(7):1187–1196. [PubMed: 19367261]

38. Gong Y, Mu D, Prabhakar S, Moser A, Musolino P, Ren J, et al. Adenoassociated Virus Serotype 9-Mediated Gene Therapy for X-Linked Adrenoleukodystrophy. Mol Ther. 2015 Jan 16.

39. Gray SJ, Matagne V, Bachaboina L, Yadav S, Ojeda SR, Samulski RJ. Preclinical differences of intravascular AAV9 delivery to neurons and glia: a comparative study of adult mice and nonhuman primates. Mol Ther. 2011 Jun; 19(6):1058–1069. [PubMed: 21487395]

40. Brody IA, Wilkins RH. Brown-Sequard syndrome. Arch Neurol. 1968 Sep; 19(3):347–348. [PubMed: 5246915]

41. Wang DB, Dayton RD, Henning PP, Cain CD, Zhao LR, Schrott LM, et al. Expansive gene transfer in the rat CNS rapidly produces amyotrophic lateral sclerosis relevant sequelae when TDP-43 is overexpressed. Mol Ther. 2010 Dec; 18(12):2064–2074. [PubMed: 20877346]

42. Bish LT, Morine K, Sleeper MM, Sanmiguel J, Wu D, Gao G, et al. Adeno-associated virus (AAV) serotype 9 provides global cardiac gene transfer superior to AAV1, AAV6, AAV7, and AAV8 in the mouse and rat. Hum Gene Ther. 2008 Dec; 19(12):1359–1368. [PubMed: 18795839]
43. Shen S, Bryant KD, Brown SM, Randell SH, Asokan A. Terminal N-linked galactose is the primary receptor for adeno-associated virus 9. J Biol Chem. 2011 Apr 15; 286(15):13532–13540. [PubMed: 21330365]
44. Snyder BR, Gray SJ, Quach ET, Huang JW, Leung CH, Samulski RJ, et al. Comparison of adeno-associated viral vector serotypes for spinal cord and motor neuron gene delivery. Hum Gene Ther. 2011 Sep; 22(9):1129–1135. [PubMed: 21443428]
45. Wang S, Samiotaki G, Olumolade O, Feshitan JA, Konofagou EE. Microbubble type and distribution dependence of focused ultrasound-induced blood-brain barrier opening. Ultrasound Med Biol. 2014 Jan; 40(1):130–137. [PubMed: 24239362]
46. Oakden W, Kwiecien JM, O'Reilly MA, Lake EM, Akens MK, Aubert I, et al. A non-surgical model of cervical spinal cord injury induced with focused ultrasound and microbubbles. J Neurosci Methods. 2014 Jun 23.235C:92–100. [PubMed: 24970578]
47. O'Reilly MA, Huang Y, Hynynen K. The impact of standing wave effects on transcranial focused ultrasound disruption of the blood-brain barrier in a rat model. Phys Med Biol. 2010 Sep 21; 55(18):5251–5267. [PubMed: 20720286]
48. O'Reilly MA, Hynynen K. Blood-brain barrier: real-time feedback-controlled focused ultrasound disruption by using an acoustic emissions-based controller. Radiology. 2012 Apr; 263(1):96–106. [PubMed: 22332065]
49. Arvanitis CD, Livingstone MS, Vykhodtseva N, McDannold N. Controlled ultrasound-induced blood-brain barrier disruption using passive acoustic emissions monitoring. PLoS One. 2012; 7(9):e45783. [PubMed: 23029240]
50. Chopra R, Curiel L, Staruch R, Morrison L, Hynynen K. An MRI-compatible system for focused ultrasound experiments in small animal models. Med Phys. 2009 May; 36(5):1867–1874. [PubMed: 19544806]
51. de Crespigny A, Bou-Reslan H, Nishimura MC, Phillips H, Carano RA, D'Arceuil HE. 3D micro-CT imaging of the postmortem brain. J Neurosci Methods. 2008 Jun 30; 171(2):207–213. [PubMed: 18462802]
52. Hakam A, Nasir A, Raghuwanshi R, Smith PV, Crawley S, Kaiser HE, et al. Value of multilevel sectioning for improved detection of micrometastases in sentinel lymph nodes in invasive squamous cell carcinoma of the vulva. Anticancer Res. 2004 Mar-Apr;24(2C):1281–1286. [PubMed: 15154661]

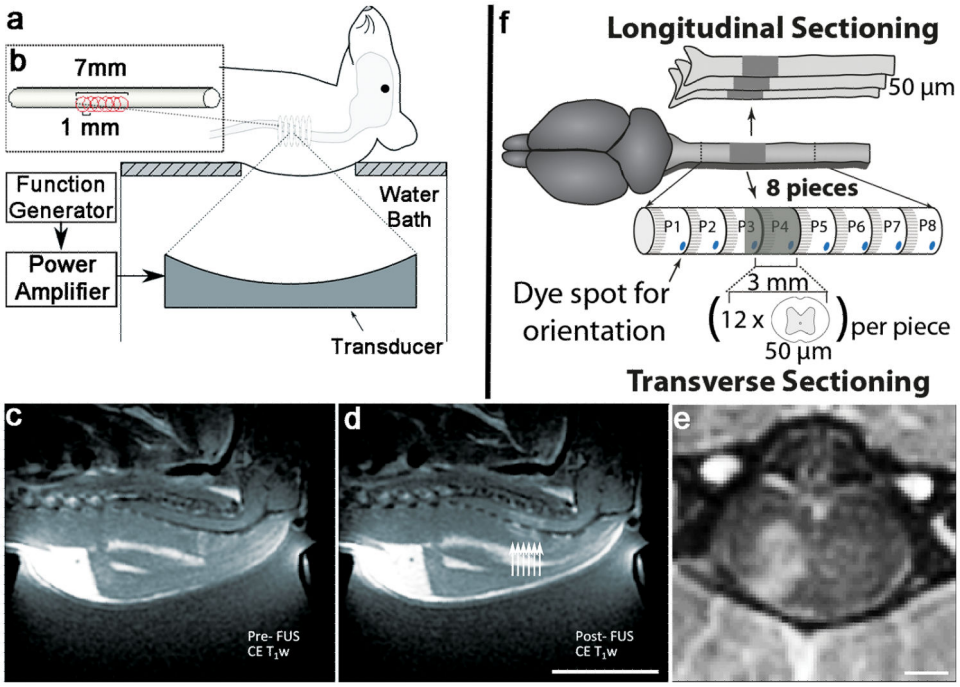

Figure 1. Experimental Setup

Each rat was positioned on the focused ultrasound (FUS) apparatus, with the target location of the spinal cord pre-identified using MRI guidance (**a**). FUS treatment was administered along 6, overlapping focal points across an approximately 7 mm section of spinal cord (**b**). T1-weighted 1.5T MRI images following gadolinium contrast agent injection were used to assess BSCB disruption by focused ultrasound (FUS). Images were obtained before (**c**, Pre-FUS) and after (**d**, Post-FUS) treatment. Enhancement (**d**, arrows) indicates successful BSCB disruption. Each arrow represents the approximate location of each ultrasound focal point. Gadolinium-enhanced 7T MRI images were taken immediately following FUS treatment, and show transverse distribution of the contrast agent within the treated side of the spinal cord (**e**). For histological assessment 13 days post-treatment, the isolated spinal cords were sectioned longitudinally, or cut into 8 pieces of 3 mm each as demonstrated in the schematic (**f**). Using previously obtained T1-weighted MRI images (**d**), the distance from the top of the spine to the area showing enhancement (BSCB disruption) was estimated. For transverse sectioning, each spinal cord was cut such that the 4th piece (P4) would represent roughly the beginning of the treated area. Thereafter, 12 transverse sections at a 50 µm thickness were cut, starting from the rostral position of the treated area, for further analysis.

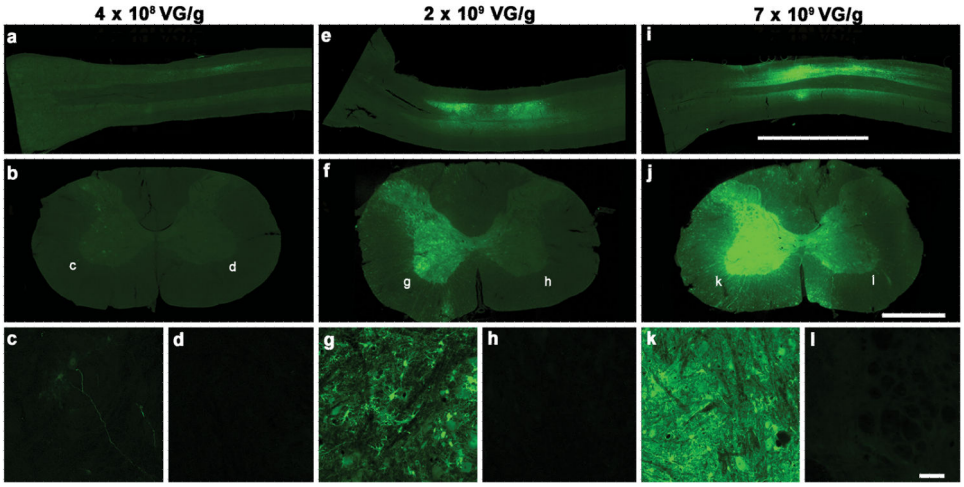

Figure 2. Gene Expression Following Unilateral MRIgFUS scAAV9-GFP Delivery to the Spinal Cord

MRIgFUS gene delivery to the spinal cord was done unilaterally at dosages of 4×10^8 VG/g (**a-d**), 2×10^9 VG/g (**e-h**), and 7×10^9 VG/g (**i-l**). The expression of scAAV9-GFP was located within the 7 mm FUS-treated area, and was largely found on the FUS-treated side of the spinal cord, as seen in both longitudinal (**a, e, i**) and transverse sections at the cervical, FUS-treated level of the spinal cord (**b, f, j**). Details at higher magnification of the FUS-ipsilateral side (**c, g, k**) and FUS-contralateral side (**d, h, l**) are also shown here. At all doses tested, viral-mediated GFP expression was mainly found on the treated side of the spinal cord, and not evident on the contralateral side (**d, h, l**). The lowest dose (4×10^8 VG/g) shows limited gene expression (**a-c**). At the middle dose (2×10^9 VG/g), GFP expression is evident (**e-g**), and remains within the treated side of the spinal cord (untreated side **h**). At the highest dose (7×10^9 VG/g), GFP expression is abundant (**i-k**) on the treated side of the spinal cord (**k**), but not on the contralateral side (**l**). Longitudinal scale bar (**a, e, i**): 6 mm. Transverse scale bar (**b,f, j**) 1 mm. Lower panels (**c, d, g, h, k, l**) scale bar: 50 μm

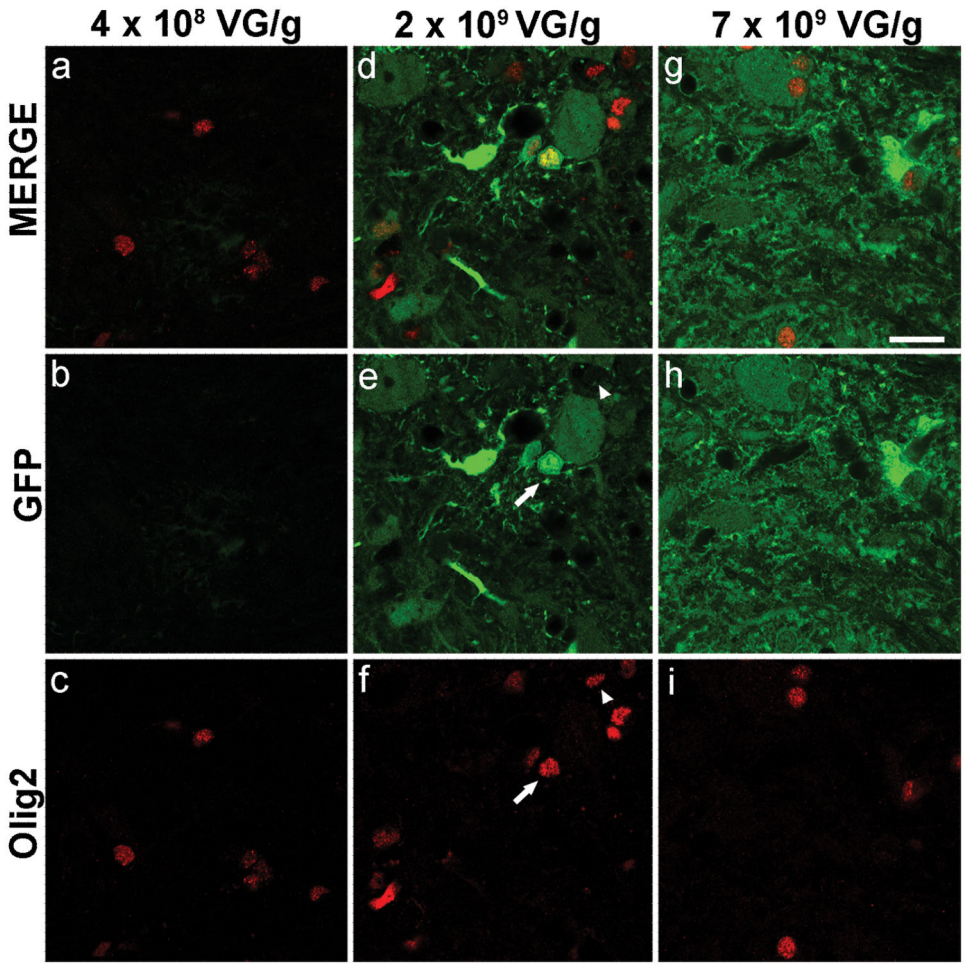

Figure 3. scAAV9-Mediated GFP Expression by Oligodendrocytes

GFP expression at the lowest dose (**a-c**) of scAAV9-GFP was not detectable in Olig2-positive cells (oligodendrocytes, red). At the middle (**d-f**) and high (**g-i**) doses of scAAV9-GFP, expression of GFP by Olig2-positive cells is evident in some cells (**e and f** arrow). At these doses, Olig2-positive cells that did not express GFP are also visible (**e and f** arrowhead). At the middle dose, and within the FUS-treated area of the spinal cord, 36% ± 3% (mean ± SD, n=4) of Olig2-positive cells expressed GFP. Scale bar: 20μm

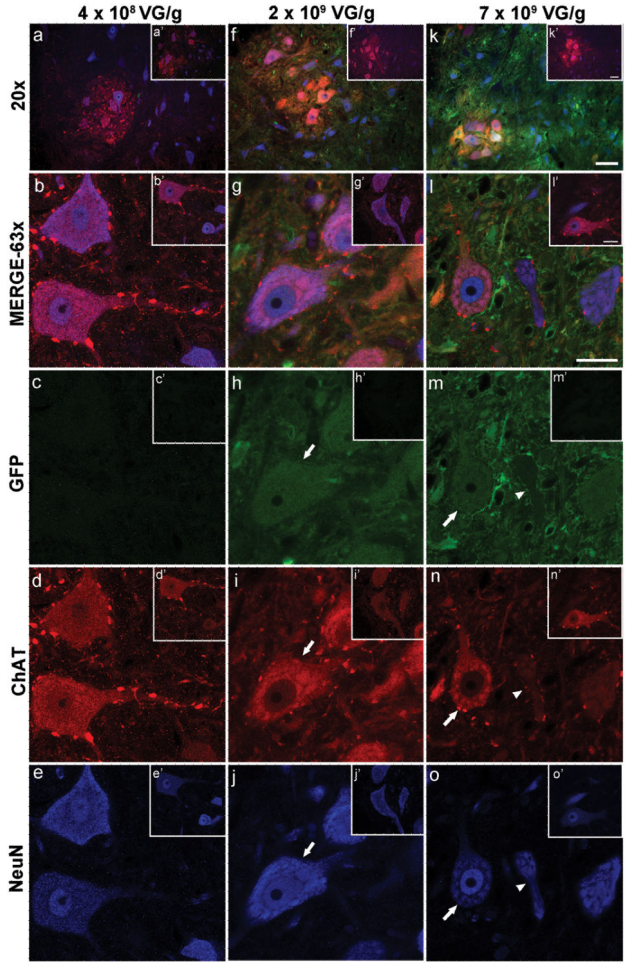

Figure 4. scAAV9- Mediated GFP Expression by Neurons

At the lowest dose ofscAAV9-GFP, GFP expression within the treated area of the spinal cord was below detection levels in ChAT (red)- and NeuN (blue)-positive cells (**a-e**). Images of the untreated side of the spinal cord also show no detectable GFP expression (**a′-e′**). At the middle dose, GFP expression was observed in ChAT- and NeuN-positive cells (**f** and **g**; **h-j**, arrow). On the contralateral side of the spinal cord, no GFP background expression was detected (**f′-j′**). At this dose, and within the FUS treated area of the spinal cord, 87% + 4% (mean + SD, n=4) of NeuN-positive cells expressed GFP. At the highest dose, most (**k** and **l**; **m-o**, arrow), but not all (**m-o**, arrowhead), ChAT- and NeuN-positive cells, expressed GFP. GFP expression on the untreated side was below detection levels (**k′-o′**). Scale bar (**a, f, k**): 50 μm; Scale bar (**b-e, g-j, l-o**): 20 μm

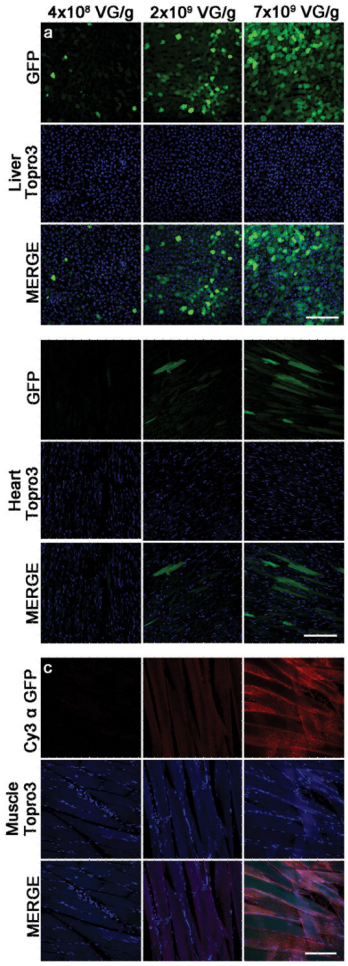

Figure 5. scAAV9-Mediated GFP Expression in Peripheral Organs

scAAV9-mediated GFP expression in the liver (**a**), heart (**b**), and muscle (**c**). GFP detection in the muscle was enhanced using an antibody against GFP coupled to Cy3 (red). Topro3 iodide nuclear stain is shown here in blue. Scale bar: 50 μm